Solar Phys
DOI 10.1007/s11207-011-9769-7

Coronal Transient Events During Two Solar Minima: Their Solar Source Regions and Interplanetary Counterparts

H. Cremades · C.H. Mandrini · S. Dasso

Received: 19 September 2010 / Accepted: 4 April 2011

Abstract In the frame of two coordinated observational and research efforts, two full solar rotations were investigated in the times of two distinct solar minima. These two campaigns were dubbed Whole Sun Month (WSM; 10 August – 8 September 1996) and Whole Heliosphere Interval (WHI; 20 March – 16 April 2008). The nearly uninterrupted gathering of solar coronal data since the beginning of the *Solar and Heliospheric Observatory* (SOHO) era offers the exceptional possibility of comparing two solar minima for the first time, with regard to the coronal transient aspect. This study characterizes the variety of outward-traveling transients observed in the solar corona during both time intervals, from very narrow jet-like events to coronal mass ejections (CMEs). Their solar source regions and ensuing interplanetary structures were identified and characterized as well, toward a global-scale description of their role in determining the heliosphere's conditions. Multi-wavelength images provided by the space missions SOHO, *Yohkoh* (only WSM), and *Solar-Terrestrial Relations Observatory* (STEREO; only WHI) and ground-based observatories were analyzed for coronal ejecta and their solar sources, while data registered by the *Advanced Composition Explorer*

The Sun–Earth Connection near Solar Minimum
Guest Editors: M.M. Bisi, B.A. Emery, and B.J. Thompson

Electronic supplementary material The online version of this article (doi:10.1007/s11207-011-9769-7) contains supplementary material, which is available to authorized users.

H. Cremades (✉)
UTN - Facultad Regional Mendoza/CONICET, Rodriguez 243, Ciudad, Mendoza M5502AJE, Argentina
e-mail: hebe.cremades@frm.utn.edu.ar

C.H. Mandrini · S. Dasso
Instituto de Astronomía y Física del Espacio, CONICET-UBA, CC. 67 Suc. 28, 1428 Buenos Aires, Argentina

C.H. Mandrini
Facultad de Ciencias y Naturales (UBA), Ciudad Universitaria, 1428 Buenos Aires, Argentina

S. Dasso
Departamento de Física (FCEN-UBA), Pab. I Ciudad Universitaria, 1428 Buenos Aires, Argentina

Published online: 12 May 2011

(ACE) spacecraft were inspected for interplanetary CMEs and magnetic clouds. Notable differences arise from the analysis of the detailed survey of events: more (fewer) ejecta during WHI (WSM), 12% (40%) were produced by active regions during WHI (WSM), and nearly no (high) deflection from the radial direction was observed during WHI (WSM). Instrumental aspects such as dissimilar resolution, cadence, and fields of view are considered in order to discern instrumentally driven disparities from inherent differences between solar minima.

Keywords Corona · Coronal mass ejections · Solar activity cycle · Interplanetary ejecta

1. Introduction

During the period 10 August – 8 September 1996, a series of coordinated efforts started with the *Solar and Heliospheric Observatory* (SOHO: Fleck, Domingo, and Poland, 1995) Joint Observing Program (JOP) 044, which eventually led to the Whole Sun Month (WSM) campaign. Its main goals included characterizing and modeling the large-scale solar minimum corona, while connecting it to *in situ* observations of the solar wind. The campaign led to a wealth of in-depth studies of the solar corona's configuration during that solar minimum (see, *e.g.*, Gibson *et al.*, 1999a, 1999b; Riley *et al.*, 1999; Zhao, Hoeksema, and Scherrer, 1999; Breen *et al.*, 1999). Twelve years later, a similarly enthusiastic motivated effort was organized, supported by several participating observatories, spacecraft, and instrument networks which ran coordinated and synoptic observations during Carrington Rotation (CR) 2068 (20 March – 16 April 2008), dubbed Whole Heliosphere Interval (WHI). Its main focus is the characterization of the Sun from its interior and throughout the heliosphere, as well as the interactions that arise with the planets, especially Earth, immersed in the solar wind. Several studies arose from the campaign, which addressed diverse aspects such as emissivity or irradiance (see, *e.g.*, Chamberlin *et al.*, 2009; Woods *et al.*, 2009), connection between heliospheric and solar phenomena (see, *e.g.*, Gibson *et al.*, 2009; Leamon and McIntosh, 2009), and highly dynamical processes (see, *e.g.*, McIntosh and de Pontieu, 2009; Gopalswamy *et al.*, 2009; Landi and Young, 2009). Out of these, only the two latter ones have directly addressed coronal mass ejections (CMEs), key drivers of space weather and therefore worthy of being thoroughly studied during this singular Carrington rotation. On the other hand, only Gibson *et al.* (2009) have explored differences and similarities between two consecutive solar minima, *i.e.* comparing WSM with WHI, though concentrating not on CMEs but on solar wind high-speed streams.

In this paper, we report on a comprehensive analysis of the ejective aspect of the Sun during two full solar rotations, taking place during two distinct but consecutive solar minima. During both WSM and WHI, strict criteria were applied in order to include all sorts of ejecta, ranging from the most impressive wide and bright CMEs down to the narrowest and faintest events. Moreover, not only white-light ejecta were considered, but also their possible *in situ* counterparts. The recent stereoscopic vision of the Sun achievable after the *Solar-Terrestrial Relations Observatory* (STEREO: Russell, 2008) was put into orbit has proven that a CME as seen from different viewing angles can reveal a very different appearance, if seen by the other spacecraft at all. At the same time, it is expected that STEREO's improved spatial coverage would lead to a higher amount of detected ejecta leaving the Sun during the WHI period. This detailed survey thus attempts to gain insight into the intrinsic dissimilarities in the ejective aspects of the past two solar minima, instrumental issues aside.

In Section 2 we discuss the criteria used to identify the solar and interplanetary events. In Section 3 we classify the different kinds of ejecta observed during these minima, while in Section 4 we list the characteristics of their associated solar source regions. Section 5

describes the interplanetary structures and solar wind characteristics found in both minima, and finally we summarize our results and conclude in Section 6.

2. Identification of Events

The proposed approach to compare the ejective aspects of these two particular solar rotations requires the inspection of the coronagraph data available during those time intervals. When available, catalogs were consulted and taken as a basis for the compilation of events. Moreover, Sterling (2010), Webb, Gibson, and Thompson (2010), and Webb *et al.* (2011) have independently compiled surveys of eruptive signatures and CMEs, which this study tends to complement. In particular, it considers all kinds of "clustered" outward-traveling material in the white-light corona as coronal ejecta. This broad criterion includes not only bright, significant CMEs but also extremely faint ones, as well as thin and narrow jets usually observed at polar latitudes.

In order to find solar wind structures potentially associated with the identified transients, *in situ* data from OMNI and from the *Advanced Composition Explorer* (ACE) were inspected, respectively, during WSM and WHI. The criteria to select interplanetary structures required the following characteristics to be present: magnetic field higher than the surroundings, low proton temperature, low plasma β, and large and coherent rotation of the magnetic field vector.

The WSM period analyzed here corresponds to the first of a series of three campaigns organized to understand the large-scale morphology, plasma properties and magnetic field configuration of the solar corona during solar minimum. These are WSM1 (10 August – 8 September 1996), originated by SOHO JOP 044; a shorter WSM2 (12 – 25 August 1998) limited by the loss of contact with SOHO in mid-'98, also referred to as the Whole Sun Fortnight; and WSM3 (18 August – 14 September 1999), corresponding to CR 1953. Since WHI was organized during the extended solar minimum preceding Solar Cycle 24, while WSM2 and WSM3 took place in the ascending phase of Solar Cycle 23, WSM1 (henceforth simply referred to as WSM) is undoubtedly the most appropriate period to be compared with WHI.

During WSM, data from the coronagraphs Large Angle and Spectrometric Coronagraph Experiment (LASCO) C1 and C2 aboard the SOHO spacecraft were inspected for ejective activity. LASCO C1 covered the heights ranging from 1.1 to 3 R_s, while LASCO C2 partially overlapped with C1 covering the range 2.2 – 6 R_s (Brueckner *et al.*, 1995), both operating 24 h a day. The provided images have a nominal pixel-to-pixel resolution of 11.2 and 22.4 arcsec, respectively, and their practical cadence during WSM rarely surpassed two images per hour. The field of view (FOV) of LASCO C2 during WSM was frequently cropped from the full 1024 × 1024 pixels to 1024 × 576 centered on the Sun. The cropped images showed the characteristic equatorial streamers of those times, but lacked coverage above the N and S poles. Possible implications arising from this and other facts will be addressed in the following section. The SOHO LASCO CME Catalog at the Coordinated Data Analysis Workshops (CDAW) Data Center[1] (henceforth CDAW Catalog) was taken as a basis to compile CMEs that occurred during WSM. The compilation was verified with the list generated by Dr. O.C. St. Cyr at the SOHO LASCO NRL website.[2] The C1 CME Catalog[3] at George Mason University was also consulted, though according to it no CME was visible in LASCO C1 for the

[1] http://cdaw.gsfc.nasa.gov/CME_list/; maintained by Seiji Yahiro (Yashiro *et al.*, 2004).

[2] http://lasco-www.nrl.navy.mil/cmelist.html; created by O.C. St. Cyr (St. Cyr *et al.*, 2000).

[3] http://solar.gmu.edu/research/cme_c1/; created by Jie Zhang.

Table 1 Sample entries of the list of ejective events and their candidate associated source regions, compiled for the WSM period. The full table can be found as an electronic supplement to this article.

Ejecta			Source Region				
Date and Time	Type	Apparent Location	Latitude	Apparent Location	Type	Remarks	
						SOHO/EIT	Yohkoh/SXT
10 Aug. 1996 09:25	CME	ENE	–	–	unknown	Possible quiescent filament behind limb	–
10 Aug. 1996 16:55	CME	WNW	−10	limb	AR	AR 7981	13:35 eruption behind W limb
...	...	...	...	...	...	...	...
8 Sep. 1996 15:16	Jet	NE		limb	CH boundary	No EIT	Bright point + jet 12:56, NE limb

duration of WSM. After inspection of LASCO C1 data we did find ejective events, although only a couple. The lack of events to deduce proper statistics made us decide not to consider LASCO C1 data in our survey.

As for coronal transient identification during WHI, once more the starting point was the SOHO LASCO CME Catalog, added to the COR1 CME Catalog at NASA GSFC[4] and the COR2-based CACTUS list of detections, at the Royal Observatory of Belgium.[5] The list of WHI events compiled by Webb *et al.* (2011) was also inspected to ensure that none of those events was missing in our selection. During this time period the inspected data were provided by the white-light coronagraphs for the inner (COR1) and outer (COR2) corona, aboard the innovative STEREO Mission (Howard *et al.*, 2008) in addition to the SOHO/LASCO C2 images. The inner COR1 coronagraph covers the range $1.4-4$ R_s with a pixel size of 7.5 arcsec, while the outer COR2 extends from 2 to 15 R_s with a pixel size of 14.7 arcsec. At the times of WHI, COR1 and COR2 recorded images with a cadence of 20 and 30 minutes, respectively. The separation of each STEREO spacecraft with respect to Earth was $\sim 23.8°$, expanding the possibilities of observing ejecta that otherwise may have not been evident in LASCO data due to directionality of Thomson scattering and projection effects.

Following the same criteria to identify white-light ejective events in the Sun's corona during both WSM and WHI, a total of 45 and 143 were, respectively, found in each of these solar rotations. An excerpt of the lists of ejective events and their candidate sources can be found in Table 1 and Table 2, while the full lists are available as supplementary material to the online article. As mentioned above, during WSM only data from SOHO LASCO was examined, while during WHI we made use of data sets compiled by five different space-borne coronagraphs: SOHO LASCO C2, STEREO COR1 (A and B), and STEREO COR2 (A and B). This fact required to exhibit statistics in a graphical fashion, as in the Venn diagram showing the overlap between the events identified in each data set (see Figure 1). In total, we identified according to our criteria in each of the inspected space-borne coronagraphs the following amount of events: 84 (LASCO); 94 (COR1-A); 113 (COR1-B); 65

[4] http://cor1.gsfc.nasa.gov/catalog/; generated by O.C. St. Cyr and maintained by Hong Xie.

[5] http://sidc.oma.be/cactus/; maintained by Eva Robbrecht (Robbrecht, Berghmans, and Van der Linden, 2009).

Table 2 Sample entries of the list of ejective events and their candidate associated source regions, compiled for the WHI period. The full table can be found as an electronic supplement to this article.

Ejecta											Source Region					
Date and Time							Type	Apparent Location			Latitude	Apparent Location			Type	Remarks
LASCO	EIT	COR1		COR2		EUVI		LASCO	COR1			EIT	EUVI			
		B	A	B	A				B	A			B	A		
20 Mar. 2008 18:30	20 Mar. 2008 15:48	20 Mar. 2008 16:05	–	20 Mar. 2008 16:35	–	–	Jet	NNE	NNE	–	65	limb	–	–	CH boundary	faint jet
21 Mar. 2008 12:06	–	21 Mar. 2008 8:45	21 Mar. 2008 5:45	–	–	21 Mar. 2008 11:56	CME	W	WNW	WNW	30	disk	–	near limb	prom quiet Sun	EUVI time is fil. disappearance in 304
…	…	…	…	…	…	…	…	…	…	…	…	…	…	…	…	…
16 Apr. 2008 4:50	16 Apr. 2008 1:48	16 Apr. 2008 3:25	–	16 Apr. 2008 4:22	–	–	Faint CME	E	E	–	0	limb	–	–	unknown	Maybe prominence eruption, too faint

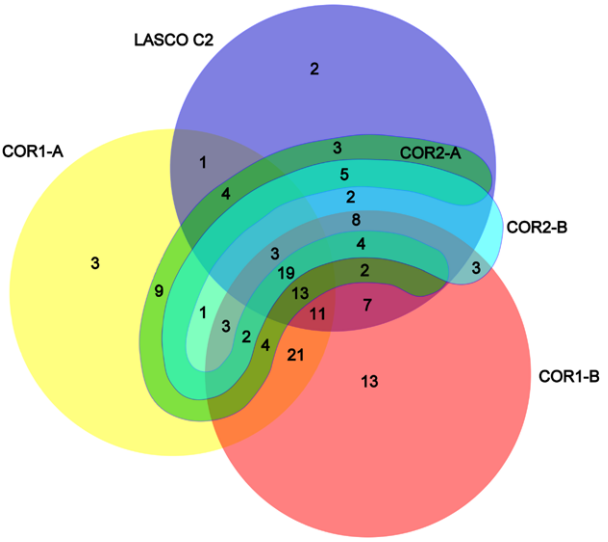

Figure 1 Venn diagram depicting the amount of ejective events detected by the five space-borne coronagraphs during the WHI period. Blue represents SOHO/LASCO C2, yellow and pink STEREO/SECCHI COR1-A and B, respectively, while green and cyan correspond to COR2-A and B, respectively. Intersection areas between different groups contain the amount of events in common.

Table 3 The amounts of white-light ejective events reported during both time periods under study. (a) Other catalogs/surveys, (b) This study.

(a)

	CDAW Catalog	COR1 Catalog	COR2 CACTUS list	Webb *et al.* (2011)
WSM	20	–	–	–
WHI	81	39	27 (A) 24 (B)	65

(b)

	SOHO LASCO C2	STEREO SECCHI COR1	STEREO SECCHI COR2	Total
WSM	45	–	–	45
WHI	84	131	65 (A) 50 (B)	143

(COR2-A); 50 (COR2-B). For comparison with other catalogs/surveys, a summary is presented in Table 3. To the 20 events catalogued by the CDAW Catalog during WSM, our study added 25 ejective events after inspection of coronal data from SOHO LASCO C2, while out of those 17 had been registered in O.C. St. Cyr's list. However, during WHI only three ejective events observed by LASCO were added to the 81 detected by the same Catalog. Different selection criteria seem to have been applied by the CDAW Catalog operators from one solar minimum to the next, especially regarding faint/narrow events. The fact that our objectives require us to follow the same identification criteria led us therefore to include several events not catalogued by the CDAW Catalog during WSM. Other data sources during WHI included STEREO's coronagraphs which widened the surveyed solar corona to $\sim 230°$. The COR1 CME Catalog reported 39 CMEs, while after following our much broader identification criteria we pinpointed 131 ejective events (113 observed by COR1-A, 94 by COR1-B, and 76 by both). Likewise, the COR2-based CACTUS list of detections reported 27 events in COR2-A and 24 in COR2-B during the same period, while we found 65

and 50, respectively, after direct inspection of running difference movies from COR2 data. These numbers correspond to a total of 85 events detected by either COR2, out of which 30 were observed by both COR2s. Only 35 events out of the 85 found by visual inspection were reported by the COR2 CACTUS list of detections, meaning a low success rate of the automated detection method, at least for COR2 during this time period. On the other hand, several events reported in COR2 CACTUS list were not identified, *i.e.* 33% corresponding to COR2-A and 30% to COR2-B either could not be discerned as ejecta from the background corona or were related to a previous event (*e.g.*, trailing outflows or general activity during or after a large CME are usually identified as separate events, as mentioned by Robbrecht, Berghmans, and Van der Linden, 2009). On the whole, our survey found 143 ejective events after inspecting and inter-relating all data sets. Conversely, the list on which Webb *et al.* (2011) based their work considered 65 events due to a different identification criterion.

Candidate solar sources for the coronal ejecta found during WSM and WHI were basically identified in the EUV, X-ray and Hα wavelengths. Candidate source regions could be recognized for 27 out of the 45 ejective events identified during WSM, while candidate sources for the WHI period could be deduced for 89 of the 143 events. Low-coronal data were inspected for signatures related to eruptions, such as eruptive prominences, flares, coronal waves, dimmings, post-eruptive loops, sigmoids, cusp formations, and bright points, the latter usually are associated with jets. Eruptive signatures found in Hα data occasionally included flares, filament disappearances, and erupting prominences. Naturally, there has to be a temporal correlation between the first detection of the CME in the coronagraph and the eruptive signature observed in the low corona and/or the chromosphere, as well as consistency between the position angle of the ejecta and its candidate source region. During WSM, images in the EUV spectral range were provided by SOHO's Extreme-UV Imaging Telescope (EIT: Delaboudinière *et al.*, 1995), observing the solar corona and transition region on the solar disk and up to a distance of 1.5 R_s, with a spatial resolution of ~ 5 arcsec. Images taken at the wavelengths of 195 Å and 284 Å were preferentially examined, with a cadence of 4 – 10 images per day per wavelength at those times. Data provided by the Soft X-ray Telescope (SXT; Tsuneta *et al.*, 1991) aboard the *Yohkoh* Solar Observatory were therefore of vital help, due to its much higher cadence of up to 40 images per day. Images at Hα wavelengths were obtained through the Global High-Resolution Hα network (http://swrl.njit.edu/ghn_web/), which holds data sets from several ground-based observatories, being the most consulted ones those from Big Bear Solar Observatory, Meudon Observatory, and Kanzelhöhe Solar Observatory. Candidate solar sources of the ejecta found during WHI were mainly identified in EUV and Hα wavelengths. In the EUV domain, SOHO/EIT images were acquired with an average cadence of 12 minutes, much higher than during WSM. Additionally, data from the Extreme-UV Imager (EUVI), part of the Sun Earth Connection Coronal Heliospheric Investigation (SECCHI) instrument suite aboard STEREO, not only provided data with improved cadence (10 and 20 minutes, respectively, for the wavelengths of 195 Å and 284 Å) and spatial resolution (which doubles that of SOHO/EIT), but also extended the Sun's longitudinal coverage to almost 230°, due to both STEREO spacecraft's separation, in opposite directions, of $\sim 23.8°$ from the Sun–Earth line. Hα data during WHI were acquired through the Global High-Resolution Hα network as well.

Following the criteria described at the beginning of this section, *in situ* data for both time periods were inspected. We could ascertain seven candidates to transient interplanetary structures in the OMNI (*Wind*) data for the WSM period, while only five could be discerned in the ACE data for WHI. Their characteristics and main properties of the background solar wind during both periods are given in Section 5.

3. Identified Types of Ejecta

The ejecta listed in Table 1 and Table 2, identified in white-light data according to the same human eye-based criteria during both investigated time periods, were classified according to their white-light appearance. The established categories are CMEs, Faint CMEs, Jets, and Streamer-swelling events. CMEs include bright, significant, "conventional" events as defined by Hundhausen *et al.* (1984), while Faint CMEs are similar events but too weak compared to the background corona, hence frequently not reported as CMEs by catalogs (see discussion in Robbrecht, Berghmans, and Van der Linden, 2009, and Figure 2(a)). Jets (see Figure 2(b)) are the white-light counterparts of transient Fe XII jets observed by Moses *et al.* (1997), also noticed by St. Cyr *et al.* (1997), and investigated by Wang *et al.* (1998) and Wang and Sheeley (2002) together with their sources at the Sun (see also Nisticò *et al.*, 2009, 2010) for recent results derived from STEREO). Streamer-swelling events refer to intermittent but persistent outward flows of material at the same position angle, commonly at equatorial streamers and likely associated with blobs, as observed by Sheeley *et al.* (1997).

Table 4 contains daily rates of ejective events, sorted according to the above categories and corrected for duty cycle. A data gap in LASCO C2 and COR1 is considered as such if longer than 1 h, since the leading edge of a fast CME traveling at $\sim 1500\ \mathrm{km\,s^{-1}}$ would

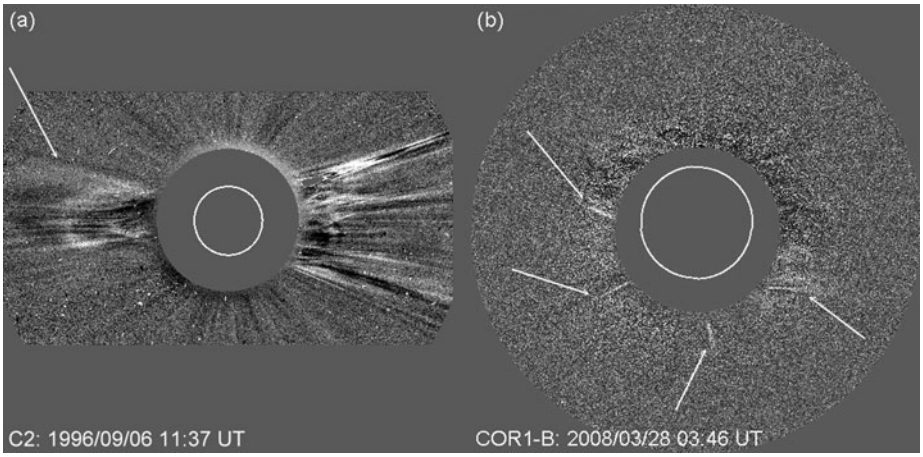

Figure 2 Samples of identified ejecta not present in online catalogs. (a) Faint CME observed by LASCO C2 during WSM, (b) Jet events observed by COR1-B during WHI. Images are courtesy of the SOHO/LASCO and STEREO/SECCHI consortia.

Table 4 Daily rates of ejective events during the two investigated time periods. Values are corrected for duty cycle and sorted into four different classes of ejecta.

	CME	Faint CME	Jet	Streamer-swelling	Total
WSM (LASCO C2)	0.49	0.25	0.56	0.28	1.6
WHI (LASCO C2)	0.98	0.76	1.31	–	3.1
WHI (COR1)	0.90	0.93	2.94	–	4.8
WHI (COR2)	0.93	0.79	1.32	–	3.0
WHI (total)	1.0	1.1	3.0	–	5.1

reach these coronagraphs' outer edge in about 0.5 h. Likewise, data gaps to be considered in COR2 need to be longer than 3 h. In spite of having added several events to those reported by the CDAW Catalog during WSM times, rates during that period are significantly lower than their analogs during WHI. The first straightforward comparison between both time periods arises from solely considering LASCO data. WHI daily rates of all considered types of ejecta at least double WSM ones, except for the case of streamer-swelling events. The latter ones seem to have been characteristic of the solar minimum preceding Cycle 23, which also exhibited a symmetric dipolar configuration. It was portrayed by well-formed polar coronal holes (CHs), the lack of low-latitude ones except for the notorious "elephant's trunk" (Biesecker *et al.*, 1999; Gibson *et al.*, 1999a; Gopalswamy *et al.*, 1999), and one streamer belt confined to equatorial latitudes delimiting the two opposite polarities. Far-limb CMEs channeled through this symmetric two-streamer arrangement may be responsible for the observation of streamer-swelling events. In contrast, during the solar minimum preceding Cycle 24 polar CHs covered smaller areas and there were several low-latitude ones spread at near-equatorial locations (Gibson *et al.*, 2009), thus denoting a less-organized distribution of open magnetic flux than during the previous solar minimum. This implies a more complex global coronal structure, lacking the presence of the symmetric two-streamer configuration observed during WSM and thus apparently hindering persistent outflows of the streamer-swelling type.

Another striking difference refers to the much larger amount of jet-like ejecta observed during WHI. It is challenging to resolve in this case whether we are in the presence of an intrinsically different solar minimum or witnessing instrumentally driven variations. Jets are on the one hand usually very fast events, and on the other hand best detected if traveling on the plane of the sky. Therefore, observational conditions during WSM were not favorable for detecting such events, first because of LASCO C2's bad cadence at the time and second because of its frequently cropped FOV at the poles. As stated in the next section, jets are commonly observed at polar position angles, so that if a polar jet was not registered by the coronagraph when it was at a low altitude from the solar limb, the possibility of detecting it at higher altitudes in the corona becomes frustrated. Additionally, ejecta traveling at a common speed of 750 km s^{-1} would take less than 0.5 h to cross the coronagraph's FOV in its narrowest portion (at the poles), which also translates into a higher number of likely undetected events. As cadence worsens, chance becomes more important when it comes to jet detection. If a jet is not traveling close to the plane of the sky, or if it travels away from it – both either in a radial or non-radial fashion, it becomes gradually harder to detect it as it travels away from the solar surface. Consequently, a high cadence is crucial to detect jets at their earliest stage of propagation, when they are still low in the corona. LASCO C2 cadence during WSM was on average of ~ 0.5 h, while during WHI it improved to ~ 20 min. This difference, together with LASCO C2's cropped FOV during WSM, likely accounts for the much higher daily jet rate during WHI. COR1 even doubles this rate, possibly because of its ability to observe at lower heights (1.4 solar radii *vs*. 2.2 for LASCO C2) and its extended coverage of solar longitudes (almost 30% higher after the separation between both STEREO S/C).

LASCO C2 Faint CMEs during WHI double as well those during WSM. The worse cadence during WSM may also play a role in this result. Frequently, faint CMEs become evident to the human eye when they are registered in consecutive images, so that the eye is guided rather by the movement of an organized structure than by the structure itself. That is to say, a still of a faint CME may not necessarily reveal its existence, though if the same event is seen to propagate in the coronagraph's FOV its presence becomes evident. Therefore, fewer images of a faint event translate into lower chances to distinguish it from

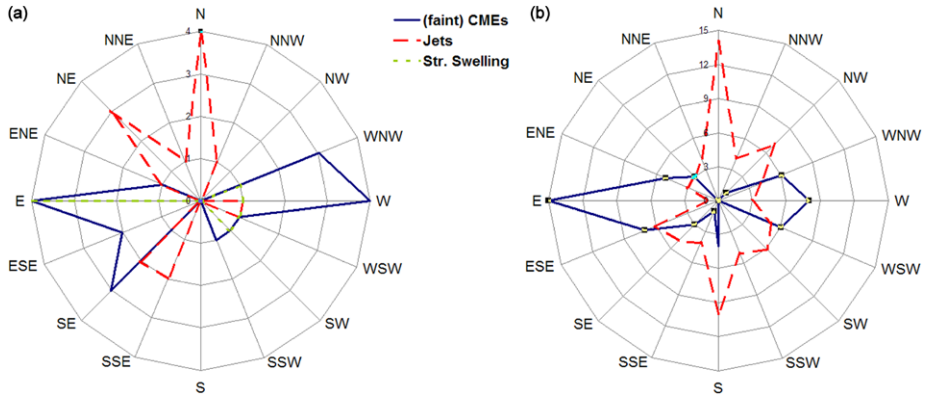

Figure 3 Apparent location of ejecta as projected in the plane of the sky for both analyzed time periods: (a) WSM, (b) WHI. CMEs and faint CMEs have been grouped into one class and are represented by continuous line, Jets are indicated by dashed line and Streamer-swelling events by dotted line.

the background corona. Another factor to bear in mind relates to the rapid diffusion of CMEs into the background brightness, as they self-similarly expand when reaching higher altitudes. As also happens with jets, faint CMEs should be brighter closer to the Sun, while at the low heights of COR1 they will be visible if additionally they propagate close to the plane of the sky.

After the analysis of daily rates of Jets and Faint CMEs, at first glance it would not appear surprising that the CME daily rate during WSM is also doubled by WHI. However it is, the "conventional" CMEs should be detected independently of the different cadence and FOV used by LASCO C2 during WSM and WHI. WSM cadence is good enough to detect even the fastest CMEs, while the cropped FOV at the poles should not be a limitation since CMEs at WSM times typically traveled close to equatorial latitudes. This comparison between observations registered by the same instrument (LASCO C2) would reveal an inherent difference between both periods under study, independent of instrumental issues.

Other differences arise when studying the apparent locations of the identified ejecta. Figure 3 depicts the location of the ejecta geometrical centers as projected on the plane of the sky, plotted in a polar-like histogram. As a histogram, it shows the number of events that have occurred at a specific location on the plane of the sky and during each time period (Figure 3(a) is for WSM and 3(b) for WHI). Streamer-swelling events appear concentrated at equatorial latitudes (*i.e.*, four events in the East and four spread around the West), as expected from the above analysis. As for jets, nearly half of them were found at polar latitudes, while the other half appeared spread at lower latitudes during both time periods. The distribution is remarkably symmetric for WHI with peaks at the poles and asymmetric towards the East for WSM. This difference is likely due to the smaller number of events detected during WSM, which are not enough to statistically reflect the locations of the full population. Jets at other than polar latitudes are found in WSM mostly due to non-radial propagation towards lower latitudes, due to deflections induced by the characteristic minimum-streamer belt at the Equator present during that period but less obvious during WHI. On the other hand, lower-latitude jets during WHI are mostly associated with low-latitude coronal holes and active regions.

Faint CMEs have been grouped together with CMEs for this analysis, given that their similar structure, though fainter, indicates the same underlying nature. No major differences

between the WSM and the WHI populations of (faint) CMEs can be observed with regard to apparent locations, which show in both cases a preference for equatorial latitudes.

4. Candidate Source Regions

Candidate solar sources for the coronal ejecta found during WSM and WHI were basically identified in the EUV, X-ray and Hα wavelengths, as mentioned above. Four types of source regions could be discerned after careful inspection of eruptive signatures in low-coronal and chromospheric data. These include: active regions (ARs), quiescent filaments, bipoles in quiet Sun locations, and bipoles within or at the boundary of coronal holes, both polar and low latitude. Samples of jet-active bipoles in coronal holes are shown in Figure 4.

Table 5 was put together after a thorough and systematic examination of identified ejecta in conjunction with low-coronal and Hα data, while the frequency of the various types

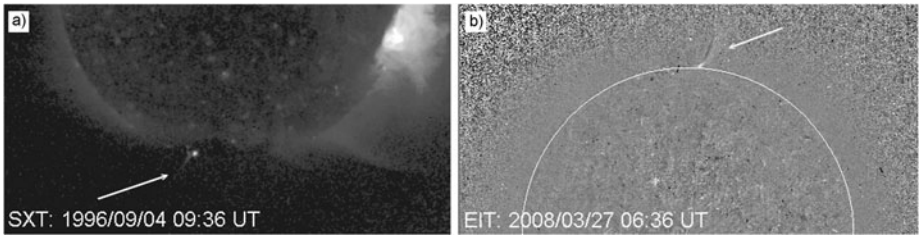

Figure 4 Examples of solar sources of jet-like events during WSM and WHI, as detected by (a) Yohkoh/SXT and (b) SOHO/EIT telescopes.

Table 5 Details of the various types of identified candidate solar sources of the ejective events found during (a) WSM, (b) WHI.

(a)

	Active Region		Bipole			Quiescent	Unidentified
	Numbered	Unnumbered	At CH boundary	Within CH	Quiet Sun	filament	
CME	5	2	0	0	0	0	7
Faint CME	2	1	0	0	0	1	3
Jet	0	1	1	4	1	0	9
Streamer swelling	3	4	0	0	0	0	1
Totals	10	8	1	4	1	1	20

(b)

	Active Region		Bipole			Quiescent	Unidentified
	Numbered	Unnumbered	At CH boundary	Within CH	Quiet Sun	filament	
CME	4	7	0	0	1	6	11
Faint CME	4	0	0	0	4	6	16
Jet	2	0	19	30	6	0	27
Totals	10	7	19	30	11	12	54

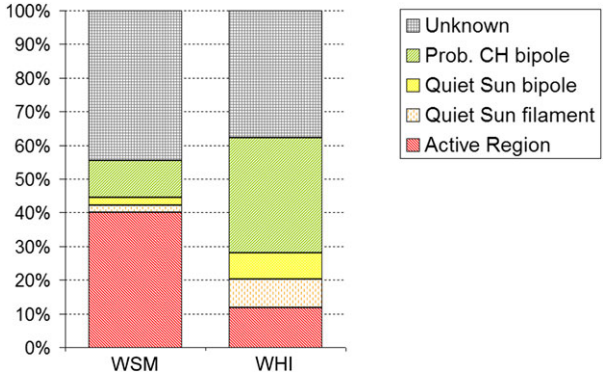

Figure 5 Proportion of the different types of source regions, candidates to be associated with the identified ejecta during both investigated time periods.

of candidate source regions during both time periods were summarized in Figure 5. Active regions appear to have played a major role as sources of white-light ejecta during WSM. Out of the 18 identified transients from ARs, nine seemed to originate from AR 7981 (denoted AR 7986 in the following rotation; compare with values found by Démoulin *et al.*, 2002), one in AR 7982, and eight in unnumbered ARs. However, during WHI all ARs as transient sources were numbered ARs (10987: two events, 10988: five events, 10989: nine events, 10990: one event).

A separate remark should be made regarding AR locations. In the WSM period, ARs were spread in a band between ±25°latitude, while bipolar regions from the next solar cycle (23) had already begun to appear at higher latitudes by May 1996. On the contrary, during WHI the "chain" of three ARs did not exceed the 12° in latitude, and only one sunspot belonging to the next solar cycle (24) had occurred at the time. Furthermore, according to the technique described by Hathaway, Wilson, and Reichmann (1994), the starting time for Cycle 24 was July 2008 with minimum in December 2008 (see D. Hathaway's Solar Cycle Prediction website at http://solarscience.msfc.nasa.gov/predict.shtml). Consequently, WHI appears to have taken place in a much deeper solar minimum than WSM, from the perspective of the photospheric magnetic field distribution. How the ejective aspect of WSM and WHI would have compared if the photospheric magnetic field distribution during both campaigns would have been similar, including the number of active regions and their locations, is still open (*i.e.*, if the time of WHI could have been deliberately chosen to be CR 2064, then, WHI could have been more comparable to WSM from the photospheric point of view, with an AR having several polarities close to the solar Equator and other few small ones spread far from the Equator and from this AR).

On the quiet Sun, quiescent prominence eruptions and filament disappearances represent a small fraction of the identified candidate sources in our survey and were equally related to CMEs and faint CMEs. On the other hand, the number of bipoles within/next to coronal holes as source candidates drastically increased during WHI with respect to WSM. This is probably due to limitations at WSM times, since SOHO/EIT was operating at a poor cadence of more than 2 h and *Yohkoh*/SXT at a cadence of 0.5 h in the best cases, clearly not enough to detect such a fast episode as the launch of a jet, except for a few fortunate cases. Bipoles not associated with CHs were scarce though existed, while the vast majority was located within CHs (WHI: 50%) or at their boundaries (WHI: 32%). Jets are undoubtedly mainly produced by bipoles, and are associated with ARs only in exceptional cases.

Unidentified source regions represent doubtlessly the largest fraction: almost half (a third) of the ejective events during WSM (WHI) could not be associated with a solar source.

Out of them, about half correspond to unidentified sources of Jets and the other half to CMEs and faint CMEs. A smaller amount of unidentified sources during WHI is likely not only related to instrumental differences between both periods, but also to the fact that STEREO could survey a larger portion of the solar sphere, thus being able to observe part of the Sun's far side.

5. Identified Interplanetary Structures

The direction of the interplanetary magnetic field (IMF) is on average in the direction of the Parker spiral (Parker, 1958; Borovsky, 2010), which is in the ecliptic plane, and near Earth forms an angle respect to the Sun–Earth direction of approximately 45° for an outward magnetic polarity (135° for an inward magnetic polarity) for a typical solar wind speed of 350 $\mathrm{km\,s^{-1}}$. However, the orientation of the IMF can suffer large deviations from this long term mean direction, mainly due to: *i*) changes in the solar wind speeds, *ii*) magnetic fluctuations, *iii*) the dynamical response to the magnetic configuration in the expanding solar wind, and the presence of non-Parkerian transients (*e.g.*, interplanetary magnetic flux ropes, ICMEs, *etc.*).

Evidence of the existence of interplanetary structures was found after inspection of OMNI (WSM) and ACE (WHI) data, following the identification criteria mentioned in Section 2. The structures found consist mainly of small flux ropes and even one magnetic cloud (MC) candidate during WHI. Table 6 summarizes the findings during the investigated time periods. Unfortunately, it was not possible to identify their potential source regions at the Sun. The small magnitude of the events, added to the fact that there were no obvious eruptions in the appropriate time windows, hindered the determination of possible associations. It is worth mentioning that the identified small flux ropes could have been locally generated within the solar wind due to magnetic reconnection across the heliospheric current sheet (Moldwin *et al.*, 2000), thus not strictly solar in origin. On the other hand, Feng, Wu, and Chao (2007) found continuous size and energy distributions between large and small flux ropes, hence suggesting there is a continuum from large to small events, which would be correspondingly associated with a broad range of CMEs, from large and bright ones to very small eruptions, likely too weak to be detected by coronagraphs.

In addition, the characteristics of the background solar wind were studied. Its IMF orientation during both WSM and WHI is shown in the form of a polar histogram in Figure 6. The IMF latitude θ_{B} angle (defined as the angle between the magnetic vector B and the

Table 6 Interplanetary structures identified from *in situ* data during both investigated time periods.

WSM		WHI	
Date	Remarks	Date	Remarks
14 Aug. 1996	flux rope (small)	22 Mar. 2008	flux rope
16 Aug. 1996	flux rope (small)	26 Mar. 2008	flux rope
17 Aug. 1996	flux rope	3 Apr. 2008	flux rope
23 Aug. 1996	flux rope	11 Apr. 2008	flux rope
25 Aug. 1996	low-field flux rope	15 Apr. 2008	long MC
2 Sep. 1996	low-field flux rope		
9 Sep. 1996	flux rope (maybe MC)		

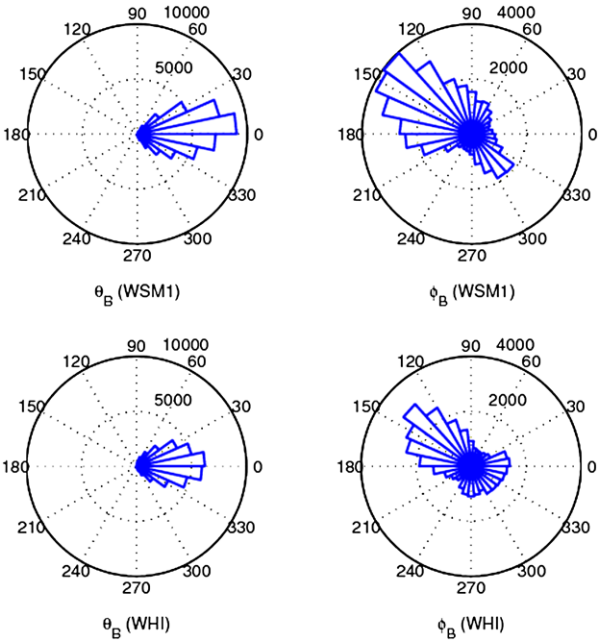

Figure 6 Angular histograms for the solar wind IMF orientation during both studied time periods. Data sources are OMNI (WSM) and ACE (WHI).

ecliptic plane, being positive when B points to North) peaks as expected at 0° in both cases, though WHI's distribution is somewhat wider. The IMF longitude ϕ_B angle (the angle between the projection of the IMF vector on the ecliptic and the Earth–Sun direction) denotes a clear preference to lie along the Parker spiral, with a tendency in favor of $\phi_B = 135°$ with respect to $\phi_B = 315°$ in both cases as well. This preference is associated with the magnetic polarity of the magnetic field in the solar wind (for outward fields $\phi_B = 135°$, for inward fields $\phi_B = 315°$). However, in the case of WSM there is a clear alignment at $\phi_B = 315°$, not evident during WHI and indicating a wider spread around the Parker's spiral in this latter period. This finding could be interpreted as crossings of the heliospheric current sheet from one side to the other but with a preference to one of them, and also with a presence of a more significant tilt of the heliospheric current sheet during WHI than during WSM.

The findings of Gibson *et al.* (2009) regarding solar wind high-speed streams (HSS) were also noticed in our analysis of WHI data. During WSM, HSS were found to be slower, less coherent and shorter in duration. Other interplanetary parameters also differed: there were longer periods of fast solar wind during WHI, likely due to the presence of more equatorial holes than during WSM. Plasma density was lower during WHI, as also found by McComas *et al.* (2008) and Issautier *et al.* (2008). Moreover, the magnetic field's absolute value in the solar wind was also somewhat smaller for WHI, indicating less open flux than during WSM (also see Smith and Balogh, 2008).

6. Summary and Conclusions

The present survey of ejective events during two specific solar rotations, occurring at the solar minima preceding Cycles 23 (WSM) and 24 (WHI), attempts to reveal inherent differences in the ejective aspect between those consecutive solar minima. Results reported by various CME catalogs were taken as a starting point to our study. In order to avoid artificially

introduced discrepancies during the selection process, we have investigated all space-borne coronagraph data for the discussed periods based on the same criteria to identify ejective events. After direct comparison of LASCO ejecta identified during WSM and WHI, it was found that WHI events almost doubled in amount those during WSM. At a first glance, this is not surprising, given the improved cadence, resolution, and longitudinal coverage achieved by the SOHO and STEREO missions during WHI. In a later step, the identified ejecta were classified according to their exhibited basic morphology into four types: streamer-swelling events, jets, CMEs, and faint CMEs. Streamer-swelling events were found during WSM above the two equatorial streamers characteristic of that solar minimum, and likely associated with far-limb CMEs that get unconditionally channeled through the organized heliospheric current sheet existing at WSM times. The number of jets and faint CMEs found was remarkably higher for WHI than for the WSM period. The small number of faint CMEs and jets found during WSM does not necessarily indicate intrinsic differences between the last two solar minima, and can at least partially be attributed to SOHO/LASCO's bad cadence at those times. WHI ejecta in the CME category outnumbered their WSM counterparts. Due to the high contrast and extension exhibited by "conventional" CMEs, instrumentally driven disparities between both periods are discounted in this latter case. Apparent location of ejecta noticeably differed from one minimum rotation to the other: in general, WHI ejecta where spread at all position angles, while WSM events had a preference for low latitudes except for a few cases at the N pole.

Source region identification of the analyzed ejective events was less ambiguous during WHI, while in WSM poor coverage and bad cadence introduced large uncertainties. It was found that $\sim 40\%$ of WSM events were produced by active regions, against only 12% of WHI ejecta. Seemingly, the complexity of the photospheric magnetic field was higher during WSM, while during WHI photospheric magnetic fields were more organized and concentrated in three active regions. According to the analysis expounded in Section 4, this fact could be related, or not, to the moment in time chosen for the WSM campaign.

The less "Parkerian" solar wind indicated by the poor alignment at $\phi_B = 315°$ during WHI can be interpreted as a sign of having crossed the heliospheric current sheet several times, with a preference to stay on one of its sides. On the contrary, WSM's alignment at 135° and 315° indicates a more symmetrical situation. Investigation of *in situ* data during both time periods yielded no significant MC or interplanetary CME at 1 AU (see also Webb *et al.*, 2011) though some candidate flux rope structures could be recognized in both rotations.

The presented findings provide insight into the past two solar minima, and in particular on the dissimilarities in their ejective aspect. The importance of considering instrumental issues when interpreting statistics was inferred during the analysis of coronal observations. Thus, it is essential to distinguish real differences inherent to these solar minima from artificial differences introduced by operational changes in same instruments, variations in the characteristics between analogous instruments, and distinct criteria of event identification used from one catalog to the other, as well as in the same catalog throughout time. On the whole, solar ejective activity during the two analyzed time periods notably differs in "conventional" CME number and deflections of polar events to lower latitudes during WSM. Mighty active regions were present during both periods, though oddly without implicating an apparent impact on geomagnetic activity: geospace parameters were exceptionally quiet during WSM, while the connection with Earth during WHI has proven to be due to recurrent high HSS (Gibson *et al.*, 2009). A fortuitous turn of events caused active regions in WSM and WHI to erupt when they were either close to the limb or on the far side of the Sun, hindering the potential geoeffectiveness of their ensuing ejecta by missing Earth.

Acknowledgements H.C., C.H.M., and S.D. are members of Carrera del Investigador Científico, CONICET. C.H.M. and H.C. acknowledge financial support from the Argentinian PIP 2009-100766 (CONICET), and PICT 1790 (ANPCyT). C.H.M. also thanks grant UBACyT X127. S.D. thanks the Argentinian grants PICT 2007-00856 (ANPCyT) and PIP-2009-00825 (CONICET), and UBACyT 20020090100264. The authors are thankful for useful discussions with S. Gibson, D. Webb and A. Sterling, as well as B. Podlipnik for providing level 1 files of LASCO/C1 data and A. Takeda for support on the SXT Movie Maker at the *Yohkoh* Legacy Data Archive. SOHO is a mission of international cooperation between ESA and NASA. EIT was funded by CNES, NASA, and the Belgian SPPS. The SOHO/LASCO data used here are produced by a consortium of the Naval Research Laboratory (USA), Max-Planck-Institut für Aeronomie (Germany), Laboratoire d'Astrophysique de Marseille (France), and the University of Birmingham (UK). The STEREO/SECCHI data used here were produced by an international consortium of the Naval Research Laboratory (USA), Lockheed Martin Solar and Astrophysics Lab (USA), NASA Goddard Space Flight Center (USA), Rutherford Appleton Laboratory (UK), University of Birmingham (UK), Max-Planck-Institut for Solar System Research (Germany), Centre Spatiale de Liège (Belgium), Institut d'Optique Théorique et Appliquée (France), and Institut d'Astrophysique Spatiale (France). The USA institutions were funded by NASA, the UK institutions by the Science and Technology Facility Council (which used to be the Particle Physics and Astronomy Research Council, PPARC), the German institutions by Deutsches Zentrum für Luftund Raumfahrt e.V. (DLR), the Belgian institutions by Belgian Science Policy Office, and the French institutions by Centre National d'Etudes Spatiales (CNES) and the Centre National de la Recherche Scientifique (CNRS). The NRL effort was also supported by the USAF Space Test Program and the Office of Naval Research. *Yohkoh* was a Japanese ISAS (present: ISAS/JAXA) mission, collaborating with NASA/US and PPARC (present: STFC)/UK, and its scientific operation was conducted by the international science team organized in ISAS. The OMNI data were obtained from the GSFC/SPDF OMNIWeb interface at http://omniweb.gsfc.nasa.gov. We are grateful to the ACE-SWEPAM and ACE-MAG teams for the data used for this work. The authors thank the referee for constructive comments on the manuscript, which helped to significantly improve this paper.

References

Biesecker, D.A., Thompson, B.J., Gibson, S.E., Alexander, D., Fludra, A., Gopalswamy, N., Hoeksema, J.T., Lecinski, A., Strachan, L.: 1999, *J. Geophys. Res.* **104**(A5) 9679.

Borovsky, J.E.: 2010, *J. Geophys. Res.* **115**, 9101.

Breen, A.R., Mikic, Z., Linker, J.A., Lazarus, A.J., Thompson, B.J., Biesecker, D.A., Moran, P.J., Varley, C.A., Williams, P.J.S., Lecinski, A.: 1999, *J. Geophys. Res.* **104**, 9847.

Brueckner, G.E., Howard, R.A., Koomen, M.J., Korendyke, C.M., Michels, D.J., Moses, J.D., Socker, D.G., Dere, K.P., Lamy, P.L., Llebaria, A., *et al.*: 1995, *Solar Phys.* **162**, 357.

Chamberlin, P.C., Woods, T.N., Crotser, D.A., Eparvier, F.G., Hock, R.A., Woodraska, D.L.: 2009, *Geophys. Res. Lett.* **36**, L05102.

Delaboudinière, J.-P., Artzner, G.E., Brunaud, J., Gabriel, A.H., Hochedez, J.F., Millier, F., Song, X.Y., Au, B., Dere, K.P., Howard, R.A., *et al.*: 1995, *Solar Phys.* **162**, 291.

Démoulin, P., Mandrini, C.H., van Driel Gesztelyi, L., Thompson, B.J., Plunkett, S., Kövári, Zs., Aulanier, G., Young, A.: 2002, *Astron. Astrophys.* **382**, 650.

Feng, H.Q., Wu, D.J., Chao, J.K.: 2007, *J. Geophys. Res.* **112**, A02102.

Fleck, B., Domingo, V., Poland, A.: 1995, *The SOHO Mission*, Kluwer, Dordrecht.

Gibson, S.E., Biesecker, D., Guhathakurta, M., Hoeksema, J.T., Lazarus, A.J., Linker, J., Mikic, Z., Pisanko, Y., Riley, P., Steinberg, J., Strachan, L., Szabo, A., Thompson, B.J., Zhao, X.P.: 1999a, *Astrophys. J.* **520**, 871.

Gibson, S.E., Fludra, A., Bagenal, F., Biesecker, D., del Zanna, G., Bromage, B.: 1999b, *J. Geophys. Res.* **104**, 9691.

Gibson, S.E., Kozyra, J.U., de Toma, G., Emery, B.A., Onsager, T., Thompson, B.J.: 2009, *J. Geophys. Res.* **114**, A09105.

Gopalswamy, N., Shibasaki, K., Thompson, B.J., Gurman, J., DeForest, C.: 1999, *J. Geophys. Res.* **104**, 9767.

Gopalswamy, N., Thompson, W.T., Davila, J.M., Kaiser, M.L., Yashiro, S., Mäkelä, P., Michalek, G., Bougeret, J.-L., Howard, R.A.: 2009, *Solar Phys.* **259**, 227.

Hathaway, D.H., Wilson, R.M., Reichmann, E.J.: 1994, *Solar Phys.* **151**, 177.

Howard, R.A., Moses, J.D., Vourlidas, A., Newmark, J.S., Socker, D.G., Plunkett, S.P., Korendyke, C.M., Cook, J.W., Hurley, A., Davila, J.M., *et al.*: 2008, *Space Sci. Rev.* **136**, 67.

Hundhausen, A.J., Sawyer, C.B., House, L., Illing, R.M.E., Wagner, W.J.: 1984, *J. Geophys. Res.* **89**, 2639.

Issautier, K., Le Chat, G., Meyer-Vernet, N., Moncuquet, M., Hoang, S., MacDowall, R.J., McComas, D.J.: 2008, *Geophys. Res. Lett.* **35**, L19101.
Landi, E., Young, P.R.: 2009, *Astrophys. J.* **707**, 1191.
Leamon, R.J., McIntosh, S.W.: 2009, *Astrophys. J.* **697**, L28.
McComas, D.J., Ebert, R.W., Elliott, H.A., Goldstein, B.E., Gosling, J.T., Schwadron, N.A., Skoug, R.M.: 2008, *Geophys. Res. Lett.* **35**, L18103.
McIntosh, S.W., de Pontieu, B.: 2009, In: Lites, B., Cheung, M., Magara, T., Mariska, J., Reeves, K. (eds.) *The Second Hinode Science Meeting: Beyond Discovery-Toward Understanding* **CS-415**, Astron. Soc. Pac., San Francisco, 24.
Moldwin, M.B., Ford, S., Lepping, R., Slavin, J., Szabo, A.: 2000, *Geophys. Res. Lett.* **27**, 57.
Moses, D., Clette, F., Delaboudinière, J.-P., Artzner, G.E., Bougnet, M., Brunaud, J., Carabetian, C., Gabriel, A.H., Hochédez, J.F., Millier, F., *et al.*: 1997, *Solar Phys.* **175**, 571.
Nisticò, G., Bothmer, V., Patsourakos, S., Zimbardo, G.: 2009, *Solar Phys.* **259**, 87.
Nisticò, G., Bothmer, V., Patsourakos, S., Zimbardo, G.: 2010, *Ann. Geophys.* **28**, 687.
Parker, E.N.: 1958, *Astrophys. J.* **128**, 664.
Riley, P., Gosling, J.T., McComas, D.J., Pizzo, V.J., Luhmann, J.G., Biesecker, D., Forsyth, R.J., Hoeksema, J.T., Lecinski, A., Thompson, B.J.: 1999, *J. Geophys. Res.* **104**, 9871.
Robbrecht, E., Berghmans, D., Van der Linden, R.A.M.: 2009, *Astrophys. J.* **691**, 1222.
Russell, C.T.: 2008, *The STEREO Mission*, Springer, New York.
Sheeley, N.R. Jr., Wang, Y.-M., Hawley, S.H., Brueckner, G.E., Dere, K.P., Howard, R.A., Koomen, M.J., Korendyke, C.M., Michels, D.J., Paswaters, S.E., *et al.*: 1997, *Astrophys. J.* **484**, 472.
Smith, E.J., Balogh, A.: 2008, *Geophys. Res. Lett.* **35**, L22103.
St. Cyr, O.C., Howard, R.A., Simnett, G.M., Gurman, J.B., Plunkett, S.P., Sheeley, N.R., Schwenn, R., Koomen, M.J., Brueckner, G.E., Michels, D.J.: 1997, In: Wilson, A. (ed.) *31st ESLAB Symp. on Correlated Phenomena at the Sun, in the Heliosphere and in Geospace* **SP-415**, ESA, Noordwijk, 103.
St. Cyr, O.C., Plunkett, S.P., Michels, D.J., Paswaters, S.E., Koomen, M.J., Simnett, G.M., Thompson, B.J., Gurman, J.B., Schwenn, R., Webb, D.F., Hildner, E., Lamy, P.L.: 2000, *J. Geophys. Res.* **105**, 18169.
Sterling, A.: 2010, In: Corbett, I.F. (ed.) *Whole Heliosphere Interval: Overview of JD16*, *Highlights of Astronomy* **15**, IAU, Cambridge Univ. Press, 498.
Tsuneta, S., Acton, L., Bruner, M., Lemen, J., Brown, W., Caravalho, R., Catura, R., Freeland, S., Jurcevich, B., Morrison, M., Obawara, Y., Hirayama, T., Owens, J.: 1991, *Solar Phys.* **136**, 37.
Wang, Y.-M., Sheeley, N.R. Jr.: 2002, *Astrophys. J.* **575**, 542.
Wang, Y.-M., Sheeley, N.R. Jr., Socker, D.G., Howard, R.A., Brueckner, G.E., Michels, D.J., Moses, D., St. Cyr, O.C., Llebaria, A., Delaboudinière, J.-P.: 1998, *Astrophys. J.* **508**, 899.
Webb, D.F., Gibson, S.E., Thompson, B.J.: 2010, In: Corbett, I.F. (ed.) *Whole Heliosphere Interval: Overview of JD16, Highlights of Astronomy* **15**, IAU, Cambridge Univ. Press, 471.
Webb, D.F., Cremades, H., Sterling, A.C., Mandrini, C.H., Dasso, S., Gibson, S.E., Haber, D.A., Komm, R.W., Petrie, G.J.D., McIntosh, P.S., Welsch, B.T., Plunkett, S.P.: 2011, *Solar Phys.*, in this issue.
Woods, T.N., Chamberlin, P.C., Harder, J.W., Hock, R.A., Snow, M., Eparvier, F.G., Fontenla, J., McClintock, W.E., Richard, E.C.: 2009, *Geophys. Res. Lett.* **36**, L01101.
Yashiro, S., Gopalswamy, N., Michalek, G., St. Cyr, O.C., Plunkett, S.P., Rich, N.B., Howard, R.A.: 2004, *J. Geophys. Res.* **109**, 7105.
Zhao, X.P., Hoeksema, J.T., Scherrer, P.H.: 1999, *J. Geophys. Res.* **104**, 9735.